TROPICAL CYCLONE RESEARCH REPORT
TCRR **0**: 1–14 (2020)
Meteorological Institute
Ludwig Maximilians University of Munich

The generalized Ekman model for the tropical cyclone boundary layer revisited: the myth of inertial stability as a restoring force

Roger K. Smith[ab1] and Michael T. Montgomery[c]
[a] *Meteorological Institute, Ludwig-Maximilians University, Munich, Germany*
[b] *Shanghai Typhoon Institute, Shanghai, China*
[c] *Department of Meteorology, Naval Postgraduate School, Monterey, California, USA*

Abstract:
We revisit the linear boundary layer approximation that expresses a generalized Ekman balance and use it to clarify a range of interpretations in the previous literature on the tropical cyclone boundary layer. Some of these interpretations relate to the reasons for inflow in the boundary layer and others relate to the presumed effects of inertial stability on boundary layer dynamics. Inertial stability has been invoked, for example, to explain aspects of boundary layer behaviour, including the frontogenetic nature of the boundary layer and its relationship to vortex spin up.
Our analysis exposes the fallacy of invoking inertial stability as a resistance to radial inflow in the boundary layer. The analysis shows also that the nonlinear acceleration terms become comparable with the linear Coriolis acceleration terms in relatively narrow, but inertially stable vortices. Estimates of the nonlinear accelerations using the linear solutions are expected to underestimate the actual contribution in a nonlinear boundary layer model, cautioning against neglecting the nonlinear terms in diagnostic or prognostic models.

KEY WORDS Tropical cyclones; boundary layer, generalized Ekman balance, inertial stability

Date: June 14, 2020; Revised ; Accepted

1 Introduction

The surface boundary layer of a tropical cyclone is known to have a strong control on the evolution of the vortex (see e.g. Braun and Tao 2000; Nolan et al. 2009a,b; Smith and Thomsen 2010; Kilroy et al. 2016 and the review by Montgomery and Smith 2017). The first three papers cited showed that vortex evolution in a numerical model is sensitive to the boundary layer parameterization employed in the model, highlighting the need for improved observations of the inner-core boundary layer. To this end, recent work applying analyses of observational data to improve forecast models has been described by Zhang et al. (2015, 2017) and Zhang and Rogers (2019).

In idealized studies, Kilroy et al. (2016) developed the concept of "boundary layer control" as part of an explanation for the long-term behaviour of tropical cyclones in the prototype problem for cyclone intensification on an f plane using a nonhydrostatic, three-dimensional numerical model, while Kilroy et al. (2017) showed that the boundary layer was an important feature of tropical cyclogenesis, even at comparatively low wind speeds.

In the context of a high resolution (at that time, $\delta x = 6$ km) simulation of Hurricane Andrew (1992), Zhang et al. (2001) set out, *inter alia*, to answer three main questions: "To what extent is the gradient wind balance model a good approximation to the local and azimuthally averaged tangential winds in an intensifying hurricane? What causes the gradient wind imbalance locally and in an azimuthally averaged state? What is the intensifying mechanism of tangential winds in the eyewall?"

Their answer to the first question was yes, to a degree within approximately 10%. However, the supergradient wind was found to play an important role in the corner flow region of the simulated storm and also in the eyewall where the air motion has an outward component. Zhang et al. found that (p106): "The radial momentum budgets show that supergradient flows and forces, even after being temporally and azimuthally averaged, are well organized from the bottom of the eye center to the upper outflow layer in the eyewall."

Zhang et al. then explained the development of the supergradient wind and spin up of the eyewall as follows (p106): " ... the development of unbalanced flows in the eyewall during the intensifying stage could be readily understood as follows. As the storm deepens, the cross-isobaric radial inflow in the marine boundary layer transports more absolute angular momentum from the hurricane environment into the eyewall region than frictional dissipation. The major radial inflow decelerates as it approaches the radius of maximum wind where the centrifugal force

[1]Correspondence to: Prof. R. K. Smith, Meteorological Institute, Ludwig-Maximilians University, Theresienstrasse 37, 80333 Munich, Germany. E-mail: roger.smith@lmu.de

exceeds radial pressure gradient force. The more the radius of the eyewall shrinks, the greater is the maximum tangential wind near the top of the marine boundary layer. Then, all the inflow air mass must ascend in the eyewall, transporting absolute angular momentum upward to spin up the tangential flow above. This upward transport of absolute angular momentum could increase significantly the local centrifugal force, thereby causing the pronounced supergradient acceleration and the development of radial outflow in the eyewall. In the present case, the supergradient acceleration occurs at the same order of magnitude as radial pressure gradient force in the vicinity of V_{max} (the maximum wind speed, our insertion), and accounts for the generation of an outflow jet near the top of the marine boundary layer. However, the local changes in tangential winds are always small due to the intense advection in the eyewall. It is evident that (a) the intensity of the radial outflow depends critically on the upward transport of absolute angular momentum, and (b) the spindown of the eyewall by radial outflow must be overcompensated by the upward transport of absolute angular momentum if the storm is to deepen. Of course, the underlying ocean (and latent heat release in the eyewall) is the fundamental energy source for the deepening of tropical cyclones."

According to the foregoing view, the evaporation of water from the underlying ocean supports a nonlinear spin up mechanism wherein the development of supergradient winds in the boundary layer of the vortex, in combination with the upward transport of absolute angular momentum from the boundary layer, plays an important role in the intensification of the storm's eyewall cloud. Similar findings were reported in idealized, but finer resolution numerical simulations by Smith et al. (2009), Persing et al. (2013) and Smith et al. (2017). The nonlinear dynamics of the vortex boundary layer and its contribution in spinning up the eyewall is discussed further from the perspective of the newly developed rotating convection paradigm by Montgomery and Smith (2017).

The upshot of these findings is that if the unbalanced processes play such a pronounced role in spinning up a tropical cyclone eyewall, a more complete understanding of the dynamics of the tropical cyclone boundary layer is certainly warranted.

One of the simplest models for a vortex boundary layer is the axisymmetric model that was first studied by Eliassen (1971) and Eliassen and Lystad (1977). Montgomery et al. (2001) pointed out that the neglected non-cyclostrophic terms in the boundary layer may become significant at higher swirl speeds, which might limit the applicability of the theory to tropical cyclones.

An analytical solution of the linear boundary layer model was obtained by Kepert (2001), who further extended the model to a moving vortex and, in a follow up study, Kepert and Wang (2001) compared predictions of the analytical solution of the linear model with a numerical solutions of a nonlinear model and used the comparison as a basis for interpreting boundary-layer behaviour.

Smith and Montgomery (2008) derived a slab version of the linear boundary layer model as one of a hierarchy of approximations for the slab model and solutions were compared with full nonlinear solutions of the slab model. They examined also the self-consistency of the linear approximation and showed that it required the smallness of a generalized vortex Rossby number. This Rossby number will generally not be small in the inner core region of a sharply peaked tangential wind profile at the top of the boundary layer. The scale analysis developed in that study was extended to the more general linear case by Vogl and Smith (2009) and the self-consistency of the linear approximation was investigated in the tropical cyclone context. These authors examined also the extent to which the accuracy of the linear approximation depends on the profile of the imposed tangential wind field at the top of the boundary layer. Consistent with Vogl and Smith (2009), Abarca et al. (2015) found that the generalized Ekman balance became invalid in both the intensifying primary eyewall region and forming secondary eyewall region.

Despite the limitations of the linear boundary layer model, it remains of intrinsic scientific interest because it is an extension of the classical Ekman boundary-layer theory to circular flow and because it may be solved analytically. In this paper we review the solutions of the linear boundary layer for broad and narrow profiles of gradient wind at the top of the boundary layer and revisit the interpretations of these solutions presented in previous studies, which are frequently invoked to explain behaviour in the nonlinear boundary layer problem also. We lay particular emphasis in reviewing these interpretations on the presumed role of inertial stability on the boundary layer structure. The concept of inertial stability has been called upon by numerous authors including three early landmark studies of the boundary layer, itself, by Shapiro (1983), Kepert (2001), Kepert and Wang (2001), the more recent study by Kepert (2017), as well as explanations for convergence in the boundary layer as part of an explanation for the physics of tropical cyclone intensification by Emanuel (2018).

2 Equations and solution in brief

In this section we summarize briefly the generalized Ekman model for a circular vortex that is in gradient wind balance above the boundary layer. The presentation follows closely that of Vogl and Smith (2009) and we focus only on the key results and interpretations pertinent to the main goals of this study.

For an axisymmetric flow expressed in cylindrical polar coordinates, the radial and tangential momentum equations for the steady boundary layer may be written as:

$$u\frac{\partial u}{\partial r} + w\frac{\partial u}{\partial z} - \frac{v'^2}{r} - \xi_g v' = \frac{\partial}{\partial z}\left(K\frac{\partial u}{\partial z}\right), \qquad (1)$$

$$u\frac{\partial v'}{\partial r} + w\frac{\partial v'}{\partial z} + \zeta_{ag} u = \frac{\partial}{\partial z}\left(K\frac{\partial v'}{\partial z}\right), \qquad (2)$$

where $v_g(r)$ is the gradient wind at the top of the boundary layer, $v' = v - v_g$ is the agradient wind, i.e. the departure of the tangential wind from the gradient wind, u and w are the radial and vertical velocity components, and K is a turbulent eddy diffusivity. It is assumed for simplicity that the radial flow above the boundary layer is zero. The quantities $\xi_g = 2v/r + f$ and $\zeta_{ag} = dv_g/dr + v_g/r + f$ are twice the absolute angular velocity and the absolute vertical vorticity of the gradient wind, respectively.

Linearization of these equations gives

$$0 = \xi_g v' + \frac{\partial}{\partial z}\left(K\frac{\partial u}{\partial z}\right), \tag{3}$$

$$0 = -\zeta_{ag} u + \frac{\partial}{\partial z}\left(K\frac{\partial v'}{\partial z}\right). \tag{4}$$

Here the linear acceleration terms have been moved to the right-hand sides of the equations, where they are then interpreted as forces per unit mass. In this form, the linear equations are seen to express everywhere a local force balance. These equations may be combined into a single fourth-order ordinary differential equation for either v' or u.

The vertical velocity in the boundary layer is determined by the continuity equation. Because the boundary layer is typically thin, density variations across it may be neglected and the continuity equation takes the approximate form:

$$\frac{\partial ru}{\partial r} + \frac{\partial rw}{\partial z} = 0. \tag{5}$$

When K is treated as constant, Equations (3) and (4) may be readily solved by taking, for example, the second vertical derivative of (3) and using (4) to eliminate $\partial^2 u/\partial z^2$ leaving a single fourth order differential equation for v', i.e.,

$$\frac{\partial^4 v'}{\partial z^4} + \frac{I^2}{K^2} v' = 0, \tag{6}$$

where, as before, $I^2(r) = \xi_g \zeta_{ag}$ is the inertial stability of the gradient flow at the top of the boundary layer. It may be verified that the solution of (6) that is bounded as $z \to \infty$ is[1]

$$v'(r,z) = v_g(r) e^{-z/\delta}(a_1 \cos(z/\delta) + a_2 \sin(z/\delta)), \tag{7}$$

where $\delta = (2K/I)^{1/2}$ is the boundary-layer scale thickness and, as shown below, a_1 and a_2 are functions of radius. The corresponding solution for u is obtained simply by substituting for v' in (4), i.e.,

$$u(r,z) = -\chi v_g(r) e^{-z/\delta}(a_2 \cos(z/\delta) - a_1 \sin(z/\delta)), \tag{8}$$

where $\chi = (\xi_g/\zeta_{ag})^{1/2}$. It follows from (7) that $v'(r,0)/v_g(r) = a_1$ and from (8), that $u(r,0)/v_g(r) = -\chi a_2$. The values for a_1 and a_2, which are functions of radius, are determined by suitable boundary conditions at the sea surface, $z = 0$.

For a turbulent boundary layer like that in a tropical cyclone, an appropriate boundary condition at the surface is to prescribe the surface stress, τ_s, as a function of the near-surface wind speed, normally taken to be the wind speed at a height of 10 m, and a drag coefficient, C_D. The condition takes the form

$$\frac{\tau_\mathbf{s}}{\rho} = K\frac{\partial \mathbf{u_s}}{\partial z} = C_D \left|\mathbf{u_s}\right| \mathbf{u_s}, \tag{9}$$

where $\mathbf{u_s} = (u, v_g(r) + v')_s$ is the wind vector at a height of 10 m. We apply a linearized form of this condition at $z = 0$, appropriate for the linearized form of the equations, to determine the constants a_1 and a_2 in (7) and (8). The derivation is as follows. The substitution of (7) and (8) into the boundary condition (9) leads before linearization to the following pair of algebraic equations for a_1 and a_2:

$$a_2 + a_1 = -\nu a_2 \sqrt{X}, \tag{10}$$

$$a_2 - a_1 = \nu(1 + a_1)\sqrt{X}, \tag{11}$$

where $X = (1 + a_1)^2 + \chi^2 a_2^2$, $\nu = C_D R_e$ and $R_e = v_g \delta / K$ is a Reynolds' number for the boundary layer. When a_1 and a_2 are small compared with unity, consistent with the linear theory, the expression for X can be linearized to give $X \approx 1 + 2a_1$, whereupon $\sqrt{X} \approx 1 + a_1$. Then the linearized form of (10) is

$$a_2 + a_1 = -\nu a_2, \tag{12}$$

$$a_2 - a_1 = \nu(1 + 2a_1), \tag{13}$$

which have the unique solution

$$a_1 = -\frac{\nu(\nu+1)}{2\nu^2 + \nu + 2}, a_2 = \frac{\nu}{2\nu^2 + \nu + 2}. \tag{14}$$

The vertical velocity, $w(r,z)$ is obtained by integrating the continuity equation (5) with respect to z:

$$w(r,z) = \frac{1}{r}\frac{\partial}{\partial r}\left[\frac{rKv_g}{\zeta_{ag}\delta}\left((a_2 - a_1)\left\{1 - e^{-z/\delta}\cos\frac{z}{\delta}\right\} + e^{-z/\delta}(a_1 + a_2)\sin\frac{z}{\delta}\right)\right]. \tag{15}$$

[1]Note that Equation (6) has solutions of the form $\exp(\alpha z)$, where $\alpha^4 = -(K^2/I^2)$ or $(K^2/I^2)\exp(\pi i + 2n\pi i)$, $i = \sqrt{-1}$ and n is an integer. Then possible values of α are $\pm\exp(i\pi/4)$ and $\pm\exp(3i\pi/4)$, or $\pm(1 \pm i)/\sqrt{2}$. The two values that lead to bounded solutions as $z \to \infty$ are $-(1 \pm i)/\sqrt{2}$.

3 Solutions

Given a radial profile of $v_g(r)$ such as one of those shown in Figure 1, together with values for K, C_D and f, it is possible to calculate the full boundary-layer solution $(u(r,z), v(r,z), w(r,z))$ on the basis of Equations (7), (8) and (15)). For illustration purposes, we choose typical values of the foregoing parameters: $K = 50$ m^2 s^{-1}, $C_D = 2.0 \times 10^{-3}$ and $f = 10^{-4}$ s^{-1}. The former two values are chosen based on recent observations of Zhang et al. (2011) and Bell et al. (2012) (see section 5.2 for an examination of solution sensitivity to K). For all these parameter values, the radial variation of the quantities ν, I^2, a_1 and a_2 are shown in the appendix for the two profiles of $v_g(r)$ in Figure 1.

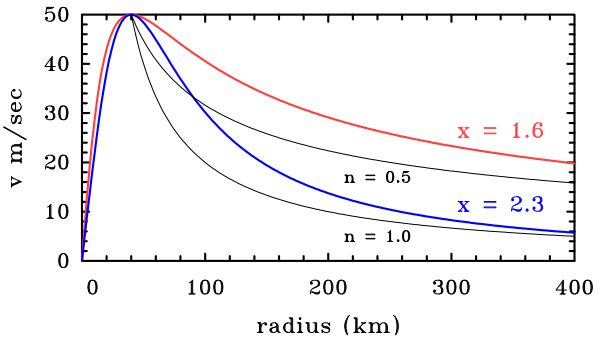

Figure 1. Tangential wind profiles as a function of radius. This profile has the form $v_g(r) = v_1 s/(1+s^x)$, where $s = s_m r/r_m$, r is the radius, r_m = 50 km and s_m and v_1 are constants chosen to make $v = v_{gm}$, the maximum tangential wind speed, when $r = r_m$. red curve has $x = 1.6$, blue curve has $x = 2.3$. The thin black reference curves are discussed in the text. These have the form $v = v_{gm}/(r_m/r)^n$, where the exponent n equals either 0.5 or 1.

As a point of reference, corresponding wind profiles for a Rankine ($v \sim r^{-1}$) and modified Rankine ($v \sim r^{-0.5}$) vortex are shown outside the radius of maximum winds. Although the narrow vortex profile decays more rapidly than the modified Rankine vortex outside of 100 km radius, the decay is still slower than that for the Rankine vortex to 400 km radius and hence inertially (centrifugally) stable for any latitude in this radial span.

Figure 2 shows radius-height cross sections of the isotachs of u, v and w below a height of 2 km for solutions with the tangential wind profiles shown in Figure 1. It shows also the radial variation of the boundary layer depth scale, δ. Note that δ decreases markedly with decreasing radius, while the inflow increases. The decrease of δ is simply related to the radial increase in the inertial stability parameter, I^2, with decreasing radius, but it ignores the likely increase in eddy diffusivity as the gradient wind speed increases. With the broader wind profile ($x = 1.6$), the maximum inflow occurs at a radius of about 85 km, 45 km outside the radius of maximum tangential wind speed above the boundary layer, r_m (panel (a)).

There is a region of weak outflow above the inflow layer with the maximum occurring at a similar radius to that of the maximum inflow. The tangential flow is slightly supergradient (i.e. $v' > 0$) in a region near the radius of maximum gradient wind r_m (panel (a)) and the maximum vertical velocity occurs within this region. The maximum vertical velocity at "large heights" peaks at a radius of about 30 km, well inside r_m (panel (c)). There is ascent in a region that expands in radius with height from about 30 km near the surface to about 190 km at a height of 2 km (panel (e)). Beyond this region there is weak subsidence, the maximum subsidence peaking at a radius of about 220 km and a height of about 500 m. The boundary layer depth scale increases from just less than 100 m near the rotation axis to just over 600 m at $r = 400$ km (panel (g)).

With the narrower wind profile ($x = 2.3$), the radial inflow is markedly stronger and somewhat deeper, but the maximum inflow occurs further outwards, near a radius of 100 km (panel (b)). The tangential flow is again slightly supergradient in a region near the radius of maximum gradient wind, r_m (panel (d)). The vertical velocity is considerably stronger (note the larger contour spacing in panel (f) compared with that in panel (e)) and the maximum ascent now occurs significantly further outwards, beyond 80 km radius, and at a significantly larger altitude, well above 1 km. The slope of the region of ascent has greatly increased and the strongest subsidence has become more confined radially and is much closer to the region of maximum ascent.

4 Interpretations

Since the linear boundary layer approximation, or generalized Ekman balance approximation, is an expression of a local force balance in a situation where the material acceleration of air parcels is negligibly small, one cannot appeal to the material acceleration terms in Newton's second law to explain the differences in behaviour for the broad and narrow profiles. Any interpretations of flow behaviour must be based on the assumption of force balance, which, of course, is reflected in the structure of the solution for the velocity components in Equations (7), (8) and (15).

4.1 Factors determining the inflow and vertical motion

In the tangential wind direction, the force balance expressed by Equation (4) is between the generalized Coriolis force, $-\zeta_{ag} u$ (minus the generalized Coriolis acceleration), which is positive, and the downward diffusion of tangential momentum, which is negative. This balance is sometimes referred to as torque balance when the equation is multiplied by the radius. It follows that, *in the linear theory*, the radial flow is determined by the tangential (*sic*) momentum equation. As discussed in section 6, this generalized Ekman balance has led a number of authors to erroneously argue that *the inflow in the nonlinear problem* is determined also by torque balance. In fact, *the inflow*

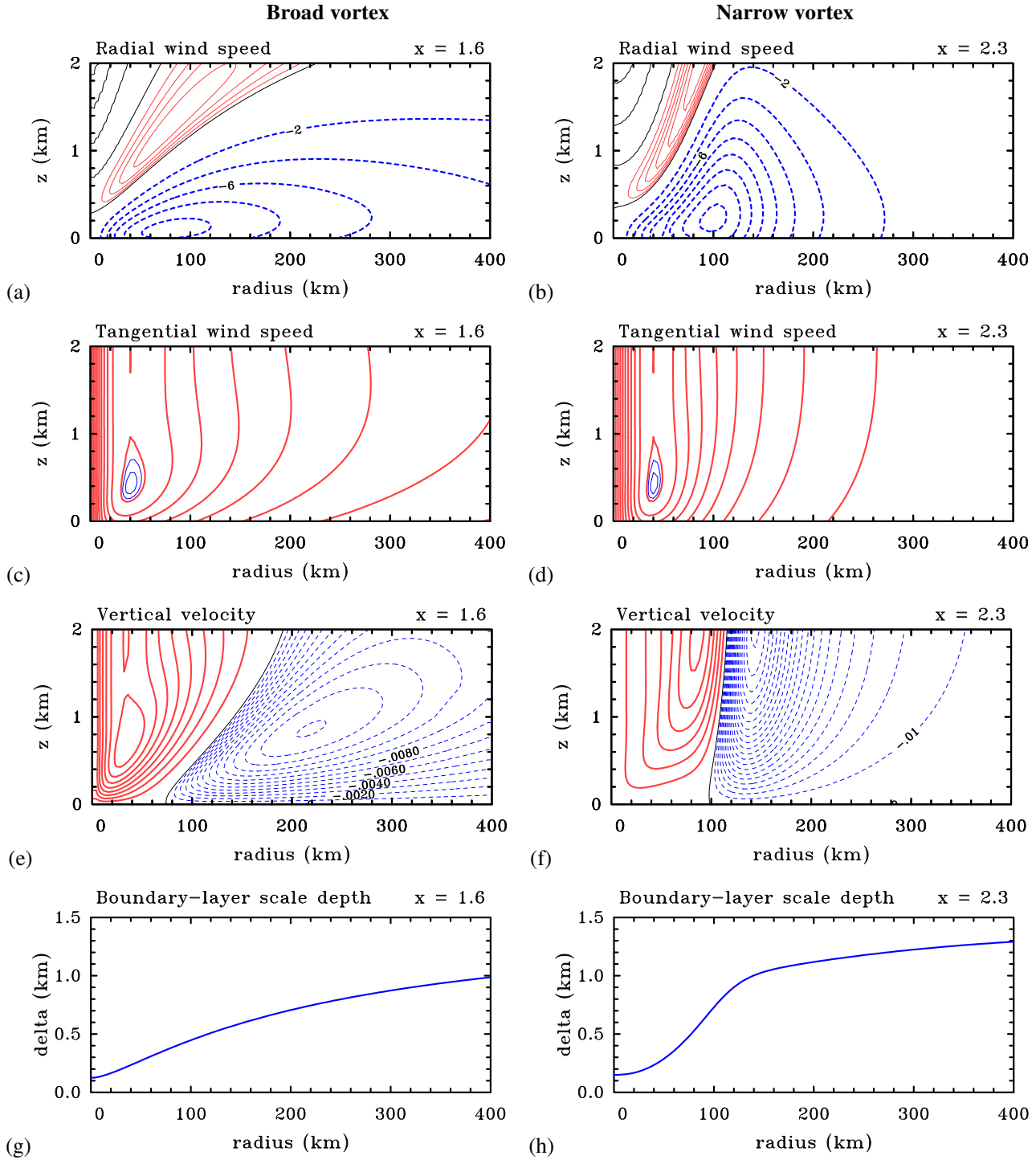

Figure 2. Isotachs of (a),(b) radial velocity u, (c),(d) tangential velocity v and (e),(f) vertical velocity w in the $r-z$ plane obtained by solving Equations (3) and (4) with the two tangential wind profiles shown in Figure 1. Left columns for the wind profile with $x = 1.6$, right columns with that for $x = 2.3$. Contour intervals: for u, 2 m s^{-1} for negative values (blue contours), 0.05 m s^{-1} for positive values (thin red contours); for v, 5 m s^{-1} for values < 50 m s^{-1} (red contours), 0.5 m s^{-1} for values > 50 m s^{-1} (thin blue contours), for w, 0.02 m s^{-1} for positive values (red contours), 0.005 m s^{-1} for negative values (thin blue contours). (g),(h) Corresponding radial variation of boundary-layer scale depth, $\delta(r)$, (unit: km).

is determined by integrating the nonlinear radial acceleration, $u\partial u/\partial r + w\partial u/\partial z - v'^2/r$, along the air parcel trajectories: see e.g. sections 5.2 and 6. Using Equation (1), the radial acceleration is equal to the generalized Coriolis force, $\xi_g v'$, plus the frictional force. Because $\xi_g v'$ is a leading-order measure of the degree of gradient wind imbalance, we refer to it here as *the agradient force*.

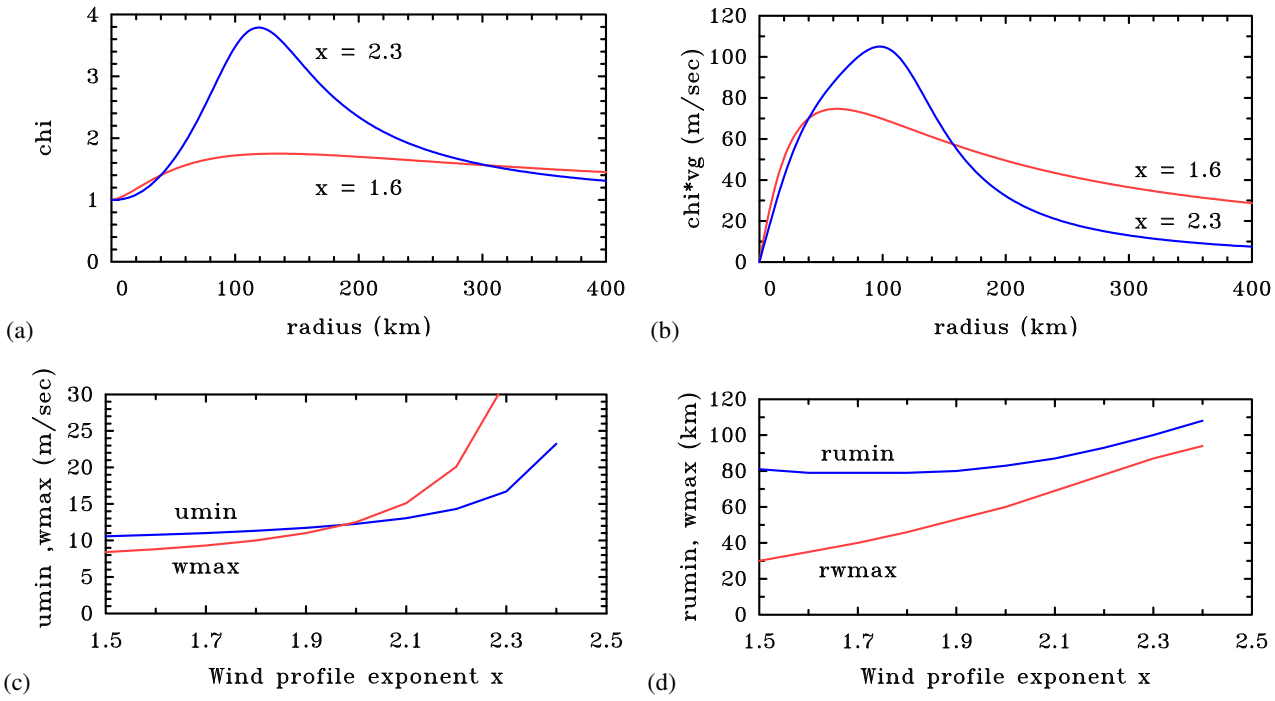

Figure 3. Radial variation of (a) χ and (b) $\chi v_g(r)$ (units: m s^{-1} for the two vortex profiles in Fig. 1. Curves for profile exponent $x = 1.6$ in red, for $x = 2.3$ in blue. Variation of (c) u_{min} (units: m s^{-1} and w_{max} (units: cm s^{-1}, and (d) r_{umin} and r_{wmax} in km with wind profile exponent x. Curves for u_{min} and r_{umin} in blue, w_{max} and r_{wmax} in red.

At a given radius, the only parameter in the solution that contains information about *the local radial variation* of the flow is the absolute vorticity, $\zeta_{ag}(r)$. In conjunction with ξ_g, ζ_{ag} enters in determining the amplitude of the radial velocity in Equation (8) through the factor $\chi v_g(r)$, where $\chi = (\xi_g/\zeta_{ag})^{1/2}$. Moreover, ζ_{ag} and ξ_g determine the inertial stability I^2, which, in turn, is a parameter involved in determining the boundary layer depth δ. It is only indirectly through the dependence of δ on I^2 that the inertial stability appears in the solution for the radial flow.

Since the coefficients $a_1(r)$ and $a_2(r)$ depend on δ and therefore on I^2 through their dependence on $\nu(r)$, it is difficult to discern the precise mathematical dependence of the radial inflow on I^2 because of the height dependence of $a_2\cos(z/\delta) - a_1\sin(z/\delta)$ in the formula for u in Equation (8). Notwithstanding this dependence, the radial profiles of χ and $\chi v_g(r)$ for the two vortex profiles shown in Figure 3 help to provide an understanding the different structure of the radial flow seen in panels (a) and (b) of Figure 2. These profiles are compared in panels (a) and (b) of Figure 3, respectively.

First note that as $r \to 0$, ξ_g is dominated by $2v_g/r$ and ζ_a is dominated by ζ so that $\chi \approx 1$. In contrast, as $r \to \infty$, both quantities are dominated by f, so that, again, $\chi \to 1$. In both vortex profiles, χ exceeds unity for all other radii, but whereas for the broad vortex profile with $x = 1.6$, the radial profile of χ is comparatively flat, for the narrower profile with $x = 2.3$ it has a sharp peak near a radius of 120 km. This peak is close to the radius of minimum ζ_{ag}, the magnitude of this minimum being smaller for the sharper profile on account of the smaller minimum of ζ_g. The radial profiles of $\chi v_g(r)$ shown in Figure 3b show also a sharper peak for the narrower vortex profile, the peak being located at a radius of 100 km, compared with only 60 km for the broader peak of the broader vortex profile.

The linear solution (Figure 2) shows that the maximum radial inflow is stronger for the narrower vortex profile (a little over 16 m s^{-1} compared with a little over 10 m s^{-1}). This property is succinctly captured by the pre-factor, $\chi v_g(r)$, plotted in Figure 3b. The stronger radial inflow at radii beyond r_{vmax} for the broader vortex profile (cf. Figure 2) is captured also by the pre-factor $\chi v_g(r)$. If the inflow was controlled primarily by the inertial stability, the radial inflow would be weaker for the broader profile. Precisely the opposite behaviour is found!

4.2 Supergradient winds in the linear solution

In section 3 we showed that the tangential flow is slightly supergradient (i.e. $v' > 0$) in a region near the radius of maximum gradient wind r_m. In the linear boundary layer solution, in regions of supergradient winds, the agradient force in the radial momentum equation is radially outwards, i.e. $\xi_g v' > 0$, and this force is exactly balanced by the upward diffusion of negative radial momentum, i.e. $\partial\tau_{rz}/\partial z < 0$, where $\tau_{rz} = K\partial u/\partial z$ is the radial stress at height z (see Equation (3)). In turn, the generalized Coriolis force associated with the diffused negative radial momentum u is balanced by the downward diffusion of tangential momentum as represented by Equation (4).

4.3 Dependence on vortex size

The broader velocity profile has a mostly larger inertial stability than the narrower profile, a fact that is reflected in a mostly shallower vertical depth scale in this case (compare panels (g) and (h) of Figure 2). For this reason, *the more radially-confined pattern of radial and vertical flow seen in panels (b) and (f) of Figure 2 compared with those in panels (a) and (e) cannot be attributed to the differences in inertial stability* when the latter is interpreted as a measure of resistance to radial motion.

The lower panels of Figure 3 summarize the changes in the maximum inflow, u_{min}, and maximum ascent, w_{max}, in the linear boundary layer solutions as the imposed vortex profile becomes narrower, i.e. the exponent x increases. It is seen that both u_{min} and w_{max} increase with x. The increase is slow at first, especially for u_{min}, but becomes more rapid as x exceeds about 2 in the case of w_{max} and about 2.2 in the case of u_{min}. The radius of maximum inflow r_{umin} changes little until x exceeds 2, whereafter it begins to increase with x until $x = 2.4$. Shortly after this value of x, the vortex profile becomes inertially unstable for a latitude of 20^o. In contrast, the radius of maximum ascent, r_{wmax}, steadily increases with x at a rate that is approximately linear from a value of only 30 km for $x = 1.6$ to a value near 95 km for $x = 2.3$.

5 Limitations of the linear theory

While providing a qualitatively correct picture of the frictionally-induced convergence in the boundary layer, a scale analysis of the boundary layer equations would suggest that the linear approximation may become poor quantitatively in a tropical cyclone strength vortex because the nonlinear acceleration terms may not be ignored: indeed, they may even dominate the linear terms (see Vogl and Smith 2009).

Figure 4 shows the structure of linear and nonlinear acceleration terms as well as their sum in the radial and tangential momentum equations, (1) and (2), respectively, for the broad and narrow gradient wind profiles shown in Figure 2. The nonlinear acceleration terms on the left-hand-side of each of these equations, calculated from the linear solutions (Equations (7), (8) and (15)), are shown in Figure 2.

The linear radial acceleration, $-\xi_g v'$, in panels (a) and (b) show a radially-outward acceleration at low levels with maximum values at the surface at radii between 30 and 40 km. This positive acceleration is equivalent to an agradient force that is of the opposite sign and in the linear solution is exactly balanced by the radial frictional force. Therefore, in this balanced perspective, the positive acceleration should not be interpreted as decelerating the boundary-layer inflow (see Equation 3). At larger heights, the radial acceleration is negative with a minimum value between 20 and 40 km radius and an altitude between 200 and 400 m.

The nonlinear radial acceleration, $u\partial u/\partial r + w\partial u/\partial z - v'^2/r$, in panels (c) and (d) is positive in the innermost region and negative beyond. For the broad gradient wind profile ($x = 1.6$) this term is relatively small in magnitude compared with the linear acceleration term, but for the narrow profile ($x = 2.3$), its magnitude is much larger and it makes a significant contribution to the total radial acceleration in panel (f).

The linear tangential acceleration, $\zeta_{ag} u$, in panels (g) and (h) is mostly negative, but in each case there are small positive values aloft. These are most noticeable above 400 m in height and inside a radius of 50 km. As noted in section 4, in the linear solution, the negative acceleration corresponds to a positive generalized Coriolis force that, in turn, is balanced by a negative frictional torque.

The nonlinear tangential acceleration, $u\partial v/\partial r + w\partial v/\partial z + uv'/r$, in panels (i) and (j) is positive for both the broad and narrow vortex profiles and in neither case is its magnitude negligibly small compared with the linear solution. Accordingly, it makes a substantial contribution to the total acceleration in panels (k) and (l).

Significantly, the nonlinear terms indicate accelerations in both the radial and tangential directions are positive compared with the corresponding linear acceleration, i.e. $-\xi_g v'$ in Equation (1) and $\zeta_a u$ in Equation (2). For this reason one might expect the linear solution to produce a weaker and broader inflow than a corresponding nonlinear solution and thereby a weaker and less concentrated region of ascent at inner radii. Not surprisingly, all the radial and tangential acceleration terms are more radially confined for the narrow vortex profile.

Since the foregoing estimates of the importance of the nonlinear terms is based on the linear solution, due to the quadratic nature of the nonlinearity, these estimates using the linear solutions can be expected to underestimate the actual contribution in a nonlinear boundary layer model (see e.g. Figures 2-4 in Smith and Montgomery 2008).

5.1 Supergradient winds in the nonlinear boundary layer

As argued by Vogl and Smith (2009), the primary reason for the departure of the linear solution from the nonlinear solution is the neglect of the radial advection of tangential momentum (or equivalently absolute angular momentum). The neglect of the vertical advection of the enhanced tangential momentum is a factor also, especially at radii near where the inflow terminates and ascends into the eyewall. The separate contributions of the radial advection and vertical advection of momentum to the total advection are illustrated in the top three rows of Figure 5 for the narrow vortex profile solution ($x = 2.3$) and with $K = 50$ m^2 s^{-1}. As in the previous section, the nonlinear terms are estimated using the linear solution and are likely to represent lower bounds on the contributions from a corresponding full nonlinear solution.

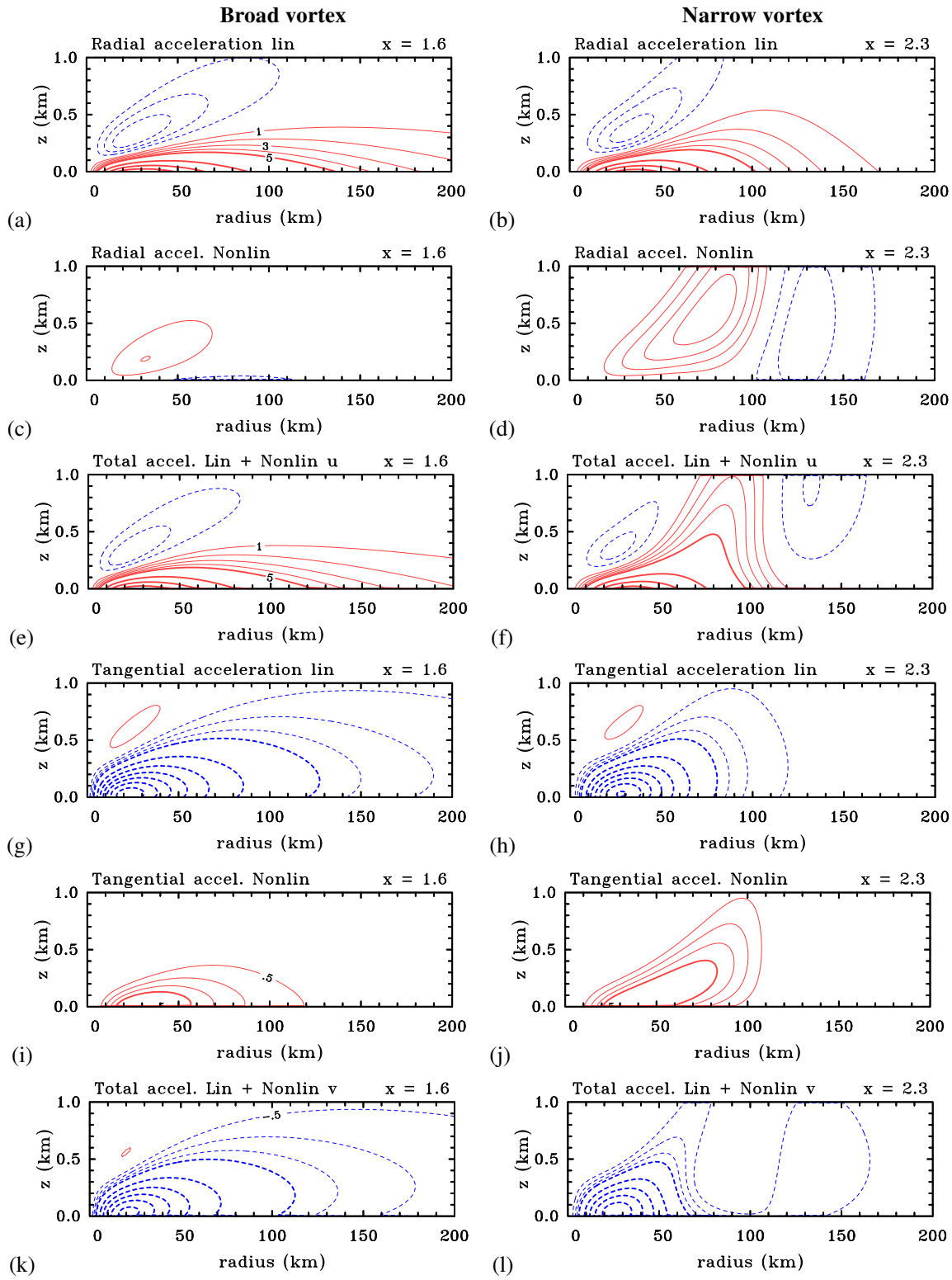

Figure 4. Isotachs in the $r-z$ plane of (a)(b) linear radial acceleration $-\xi v'$ in Equation (1), (c),(d) nonlinear radial acceleration $u\partial u/\partial r + w\partial u/\partial z - v'^2/r$, with the nonlinear term calculated from the linear solution to Equations (7) and (8), (e),(f) total radial acceleration (linear + nonlinear) $u\partial u/\partial r + w\partial u/\partial z - v'^2/r - \xi v'$, (g),(h) linear tangential acceleration $\zeta_a u$ in Equation (2), and (i),(j) nonlinear tangential acceleration $u\partial v'/\partial r + w\partial v'/\partial z + uv'/r$ with the nonlinear term calculated from the linear solution to Equations (7) and (8), (k),(l) total tangential acceleration (linear + nonlinear) $u\partial v'/\partial r + w\partial v'/\partial z + uv'/r + \zeta_a u$. Left columns for the tangential wind profile in Figure 1 with $x = 1.6$, right column with the profile for $x = 2.3$. Contour intervals for radial terms: 5 m s^{-1} h^{-1} (thick contours), 1 m s^{-1} h^{-1} (thin contours); for tangential terms: 2 m s^{-1} h^{-1} (thick contours), 0.5 m s^{-1} h^{-1} (thin contours). Positive values red, solid; negative values blue, dashed.

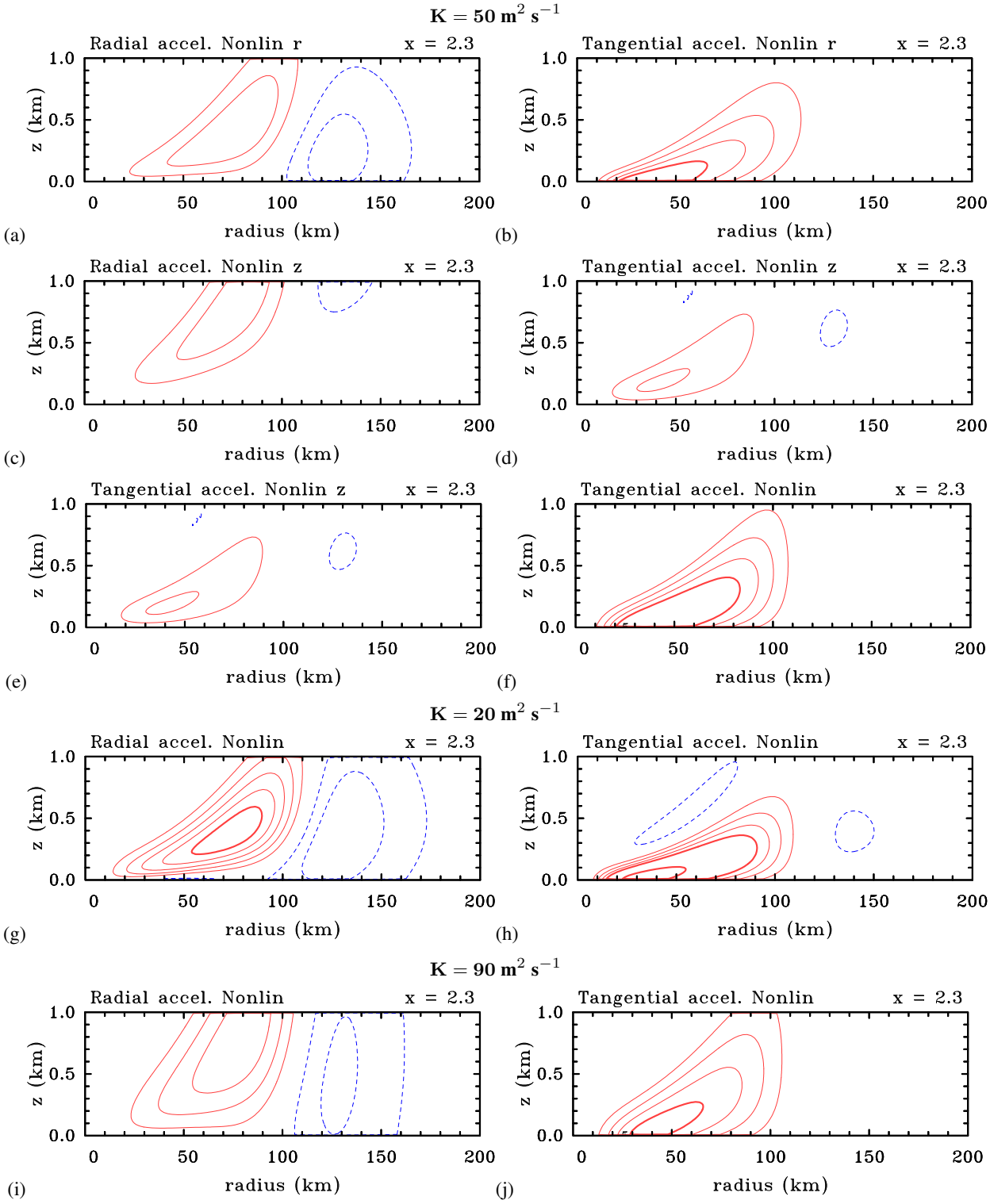

Figure 5. (a)-(f): Isotachs in the $r-z$ plane of the contributions to the nonlinear radial and tangential acceleration terms and the sum of these contribution in the calculation with $K = 50$ m^2 s^{-1}. All terms are calculated from the linear solution. (a) radial advection contribution including the perturbation centripetal acceleration, $u\partial u/\partial r - v'^2/r$, (c) vertical advection contribution $w\partial u/\partial z$, to (e) the nonlinear radial acceleration $u\partial u/\partial r + w\partial u/\partial z - v'^2/r$. (d) radial advection contribution $u\partial v'/\partial r + uv'/r$, (e) vertical advection contribution $w\partial v'/\partial z$ to (f) the nonlinear tangential acceleration $u\partial v'/\partial r + w\partial v'/\partial z + uv'/r$. (g) nonlinear radial acceleration and (h) nonlinear tangential acceleration based on the linear solution with $K = 20$ m^2 s^{-1}. (i) nonlinear radial acceleration and (j) nonlinear tangential acceleration based on the linear solution with $K = 90$ m^2 s^{-1}. Contour intervals for radial terms: 5 m s^{-1} h^{-1} (thick contours), 1 m s^{-1} h^{-1} (thin contours); for tangential terms: 2 m s^{-1} h^{-1} (thick contours), 0.5 m s^{-1} h^{-1} (thin contours). Positive values red, solid; negative values blue, dashed.

The left column of Figure 5 refers to the nonlinear terms in the radial momentum equation and the right column to those in the tangential momentum equation. In the radial momentum equation, the contributions from radial and vertical advection are positive inside a radius of about 100 km and negative beyond this radius, with maxima a little over 2 m s^{-1} h^{-1}. Further, the positive values are comparable in magnitude in both contributions. In the tangential momentum equation, the radial advection has a maximum value exceeding 2 m s^{-1} h^{-1}, which is approximately twice the maximum of the vertical contribution (i.e., just over 1 m s^{-1} h^{-1}).

The radial advection of perturbation tangential momentum shown in Figure 5b encapsulates the nonlinear boundary layer spin-up mechanism as articulated most recently by Smith and Montgomery (2017), pp1501-1502. This mechanism was already anticipated in the early studies of Anthes (1971, 1974), Shapiro (1983) and Zhang et al. (2001). The mechanism accounts for the generation of much stronger supergradient winds inside and near the radius of maximum gradient wind than those that occur in the linear boundary layer solution. In a related study based on an idealized numerical simulation, Abarca et al. (2015) showed that the supergradient winds in both the intensifying primary eyewall region and forming secondary eyewall region were so large that the generalized Ekman balance would be a poor approximation (see their Figures 3 and 4 and accompanying discussion).

5.2 Dependence on K

In footnote 3 of their paper, Kepert and Nolan (2014) wrote: "Some may be surprised by the satisfactory performance of the linearized model, given that Vogl and Smith (2009) analyzed a linearized tropical cyclone boundary layer model similar to that of Kepert (2001) and claimed that the removal of the nonlinear terms was not consistent. These terms are certainly important, as shown by Kepert (2001), Kepert and Wang (2001), and Kepert (2013). However, Vogl and Smith's analysis exaggerates their importance, because they use a very small value of the diffusivity, $K = 10$ m^2 s^{-1}, which leads to a boundary layer that is too shallow. The inflow becomes too strong to maintain the necessary advective flux of absolute angular momentum to balance its frictional destruction at the surface (Kepert 2013). Thus, the nonlinear advection terms are exaggerated."

Since the publication of Vogl and Smith (2009), some observational guidance has emerged on the vertical eddy diffusivities in tropical cyclones (Zhang et al. 2011, Figure 10). Typical values of K given by Zhang et al. are on the order of 50 m^2 s^{-1}, although, there is considerable scatter in the observations, which show a dependence also of K on mean wind speed. The value chosen here is within the middle range of observed values with the lowest values around 10 m^2 s^{-1} and highest values around 100 m^2 s^{-1}, while the value used by Vogl and Smith op. cit. is at the lower end of the range, though not entirely unrealistic. A more substantial issue would be the assumption of a constant value for K at all radii and therefore all wind speeds. The variation of K with radius is certainly an important feature to represent in a realistic forecast model, but this lies outside the scope of the current study.

To investigate the dependence of the nonlinear terms on the value of K, we show in the last two rows of Figure 5 cross sections of these terms for $K = 20$ m^2 s^{-1} (panels (g) and (h)) and $K = 90$ m^2 s^{-1} (panels (i) and (j)), which should be compared with those for $K = 50$ m^2 s^{-1} in the middle row, panels (e) and (f). While supporting Kepert's supposition that the magnitude of the nonlinear terms will increase with decreasing K, one cannot safely claim that the values in Vogl and Smith (2009) are exaggerated as those estimates, like the ones in Figure 5, are likely to be lower estimates for these terms (see section 5). The foregoing analysis shows that the findings of Vogl and Smith are robust.

It is pertinent to analyse the penultimate sentence in the foregoing quotation from Kepert and Nolan (2014): "The inflow becomes too strong to maintain the necessary advective flux of absolute angular momentum to balance its frictional destruction at the surface (Kepert 2013)". This sentence is *non sequitur* because it does not say to what "the inflow" refers. If it refers to the inflow in the linear solution, then it cannot be "too strong to maintain the necessary advective flux of absolute angular momentum to balance its frictional destruction", since it is from this constraint that the inflow is determined. If, instead, it refers to the inflow in the nonlinear solution (which was not calculated by Vogl and Smith 2009), it would be an example of the misleading invocation of torque balance to explain the reason for inflow in the *nonlinear* boundary layer.

6 Confusion in the literature

The foregoing exposition of linear boundary layer theory provides a basis for clarifying a range of interpretations in the previous literature on the tropical cyclone boundary layer. Some of these interpretations relate to the presumed effects of inertial stability on boundary layer dynamics as invoked, for example, by Shapiro (1983), Kepert and Wang (2001), Zhang et al. (2001) and Kepert (2017) to explain aspects of boundary layer behaviour, and by Emanuel (2018) to explain the frontogenetic nature of the boundary layer and its relationship to vortex spin up.

6.1 Reasons for the boundary layer inflow

As pointed out in section 4.1, the inflow in the nonlinear boundary layer arises because of the agradient force in the radial momentum equation. In contrast, in the linear problem, the agradient force is exactly balanced by the frictional force in the radial direction. In the tangential

direction, the generalized Coriolis acceleration, $-\zeta_{ag}u$, is exactly balanced by the frictional force, which is equivalent to an assumption of torque balance. In this case, the radial flow is determined by the tangential momentum equation. On the assumption that the nonlinear boundary layer flow does not deviate greatly from torque balance (Willoughby 1988, p186[2]) a number of authors have been led to erroneously argue that *the inflow in the nonlinear problem* is determined by torque balance also.

The issues involved are subtle. Even if the degree of imbalance expressed by the agradient force and friction is small, it cannot be inferred that the imbalance can be neglected. For one thing, the effects of a small net inward force can accumulate over a hundred kilometres or more in radius, just as the buoyancy force based on a few degrees of temperature excess in a cumulonumbus cloud can lead to a significant updraught strength. For another thing, torque balance cannot account for the development of significant supergradient winds that have been found in observations (Kepert (2006); Sanger et al. (2014); Montgomery et al. (2014)) and their contribution to the nonlinear deceleration of the boundary layer inflow inside the radius of maximum gradient wind speed.

As one illustration of the foregoing issues, Kepert and Wang *op. cit.* note on the first page of their paper that "vertical diffusion could maintain inflow in the presence of a weakly supergradient jet in the upper boundary layer". The reader is left to work out what is being diffused (presumably some component of horizontal momentum), and the authors do not say how the diffusion "maintains the inflow" nor do they explain the role of the "weakly supergradient jet", which is in the tangential direction and not the radial direction. It would appear that here they are invoking torque balance, even for the fully nonlinear problem. As shown above, this would be incorrect.

While acknowledging the radial force imbalance as the source for the radial acceleration in their statement on p2493: "From a Lagrangian point of view, the imbalance in the adjustment terms directly accelerates the air parcels inward", Kepert and Wang return to invoking torque to describe the nonlinear behaviour of the radial inflow for the inertially stable and neutral cases. For example, on p2493: sentence beginning "Our analysis so far has strongly suggested that, ... "; p2495: sentence beginning: "In summary, frictional destruction of ...", and p2500: paragraph beginning "The spatial distribution of the jet ... ".

6.2 The presumed role of inertial stability

The concept of inertial (or centrifugal) stability of an axisymmetric vortex with tangential wind distribution $v(r)$ relates to the restoring force that acts on a fluid parcel at some radius when it is displaced radially through a small distance Δr. If the vortex is situated on an f plane, the restoring force per unit mass $F = -I^2\Delta r$, where I^2 is defined just below Equation (6) (Rayleigh 1917). It is unclear how this concept relates to the vortex boundary layer, where on account of friction, there is already a nonzero agradient force acting on all fluid parcels.

The so-called inertial stability, I^2, appears as a coefficient in the Sawyer-Eliassen equation for the streamfunction of a slowly-evolving balanced vortex, another important coefficient being the static stability N^2 characterizing the vertical restoring force per unit mass for a vertical displacement, Δz, of a fluid parcel (Willoughby 1979). Based on the work of Eliassen (1951), Shapiro and Willoughby (1982) pointed out that the circulation induced by a point source of heating or momentum in such a balanced flow is confined in radius if $I^2 >> N^2$ and confined in the vertical if $N^2 >> I^2$. Kepert and Wang explained the strength of the inflow in their nonlinear boundary layer solutions using this balance framework. It is again unclear that balance dynamics can be applied to the boundary layer. For one thing, the linear boundary layer solution expresses a rather different balance (i.e. generalized Ekman balance) compared with thermal wind balance assumed by Shapiro and Willoughby. For another thing, the existence of infow in the frictional boundary layer is fundamentally a consequence of radial force imbalance.

Possibly the first reference to the presumed role of inertial stability as a restoring force in the boundary layer was that by Shapiro (1983). When describing the axisymmetric nonlinear boundary layer response to an imposed radial pressure gradient forcing, Shapiro wrote on p1988: "The inertial "wall", evidenced by the rapid increase in vorticity (ζ_o), just inside r_{max} (the radius of maximum tangential wind speed, our insertion) leads to the rapid deceleration of u_o (the radial velocity, our insertion), and strong boundary layer convergence".

Kepert and Wang (2001) use a similar argument, stating on p2493: " ... the radius of maximum winds is a highly favorable location for low-level jet occurrence, due to the sudden increase in inertial stability allowing a strong updraft there, and the increased radial gradient of M_a (the absolute angular momentum of the gradient wind: our insertion)". The argument is similar to that of Shapiro because the radial gradient of M_a is proportional to the absolute vorticity.

Referring to the fact that the peak axisymmetric updraft typically falls a few kilometers within the radius of maximum tangential wind, Kepert (2017) argues on p3319 that "Essentially, this displacement is a measure of the overshoot as the inflowing near-surface air encounters the greater inertial stability of the gradient wind at the eyewall and decelerates".

In a similar vein, Emanuel (2018) argued on p15.15 of his monograph on tropical cyclones: " ... the boundary layer

[2]There, Willoughby writes: "Although the wind may be supergradient where the boundary-layer inflow decelerates and turns upwards into the eyewall, the role of the imbalance in the secondary circulation has been exaggerated."

near the radius of maximum winds is strongly frontogenetical, with convergence of the Ekman boundary layer flow guaranteed by the large radially inward increase of inertial stability as the vorticity rapidly increases inward".[3]

All the foregoing arguments would appear to be based on torque balance. As noted earlier, if one assumes that, to a first approximation, linear Ekman balance holds in the boundary layer, the radial velocity given by Equation (4)[4] is inversely proportional to ζ_{ag}. It is evident that all the authors are conflating absolute vorticity with inertial stability. While the absolute vorticity is a mathematical component of inertial stability, the two concepts have different physical meanings as well as different dimensions. Although it is true that, in cases where the vortex core is approximately in solid body rotation, inertial stability and absolute vorticity both show a sharp increase with decreasing radius near and inside the radius of maximum gradient wind, neither quantity can be interpreted physically as a resistance to radial motion in the boundary layer.

Further confusion relating to the role of inertial stability in the boundary layer is found in Zhang et al. (2001) who write on p101: "Clearly, *it is the centrifugal force (or inertial stability) that prevents the low-level radial inflow from reaching the eye, and vents the air from the bottom of the eye to maintain the mass balance*". While their arguments regarding the role of the centrifugal force are broadly correct (see paragraph below), these authors conflate "inertial stability" with the centrifugal force.

In the nonlinear boundary layer, the rapid deceleration of the inflow near and inside the radius of maximum gradient wind is due to the positive agradient force, which is associated, mostly through the dominance of the centrifugal force, with the development of supergradient winds in that region (e.g. Anthes 1974, p506, Zhang et al. 2001, sec. 4, Nguyen et al. 2002, sec. 5b, Smith and Vogl 2008, p342, Smith et al. 2009). Thus, we would argue that it is fallacious to invoke inertial stability to explain the rapid deceleration of the inflow in the boundary layer. The foregoing examples are only a few of the instances we found in the literature where inertial stability has been invoked to explain boundary layer behaviour, an indication that such misleading interpretations have become entrenched.

[3]Strictly speaking, this reasoning, like that of Kepert and Wang (2001) cited above, is not entirely sound. This is because, while the absolute vorticity on the left-hand side of torque balance increases with decreasing radius, the quadratic drag on the right-hand side of torque balance increases with decreasing radius also. According to torque balance, the radial inflow is determined by the ratio of the tangential drag per unit depth to the absolute vertical vorticity, both of which increase with decreasing radius. Although one might surmise that the increase in absolute vorticity is more rapid than that of the drag per unit depth, it is not obvious which effect wins, except for the special case of a Rankine vortex ($v \sim r^{-1}$). However, torque balance becomes invalid in the case of a Rankine vortex (e.g. McWilliams 1971; Kepert 2001).

[4]If Equation (4) is integrated vertically over the depth of the boundary layer, the mean inflow is seen to be proportional to the surface stress in the tangential direction and inversely proportional to the product of the boundary layer depth times the absolute vorticity of the gradient wind (e.g. Willoughby 1995, Equation (2.11)).

7 Conclusions

We have reviewed the linear theory of a turbulent vortex boundary layer in the context of tropical cyclones and have examined in detail two solutions of the linear boundary layer equations for broad and narrow gradient wind profiles that have the same radius of maximum tangential wind speed. We examined further the integrity of these solutions by using them to estimate the nonlinear terms that were neglected in their derivation. These terms are not negligible for the narrower vortex profile. The analysis shows that the linear approximation is best for the broader gradient wind profile. It shows also that the structural differences between the two solutions cannot be explained on the basis of inertial stability arguments.

We have argued that, even if the degree of radial force imbalance in the boundary layer is small, its effects cannot be simply dismissed. The reason is that the effects of a small, but persistent net inward force can accumulate over a hundred kilometres or more in radius. In particular, it is fallacious to attribute inflow in the nonlinear boundary layer to torque balance, because it would be determined then by the tangential (*sic*) momentum equation. We pointed out that, in the tangential direction, torque balance *cannot* account for the development of supergradient winds and their contribution to the rapid deceleration of the boundary layer inflow inside the radius of maximum gradient wind speed. These effects are intrinsically nonlinear and require consideration of both horizontal momentum equations.

We have examined some previous interpretations of both linear and nonlinear boundary layer behaviour, which we believe are deficient. In particular, we have examined arguments about boundary layer behaviour that invoke inertial stability ideas borrowed from balance vortex theory and have questioned the application of such ideas when applied to the vortex boundary layer.

Acknowledgements

This paper was largely written while the first author was a visiting scientist at the Shanghai Typhoon Institute in November 2019. Thanks go to Drs. Jie Tang and Shengming Tang for their warm hospitality during this visit and for providing an environment conducive for research. MTM acknowledges the support of NSF grants AGS-1313948 and IAA-1656075, ONR grant N0001417WX00336, and the U. S. Naval Postgraduate School. The views expressed herein are those of the authors and do not represent sponsoring agencies or institutions.

Appendix: Radial variation of ν, I^2, a_1 and a_2

Figure 6 shows the radial variation of the quantities ν, I^2, a_1 and a_2 that appear in the solution to the linear boundary layer problem. These quantities are calculated with the parameter values given at the start of section 3 and the two vortex profiles defined therein. It is seen that

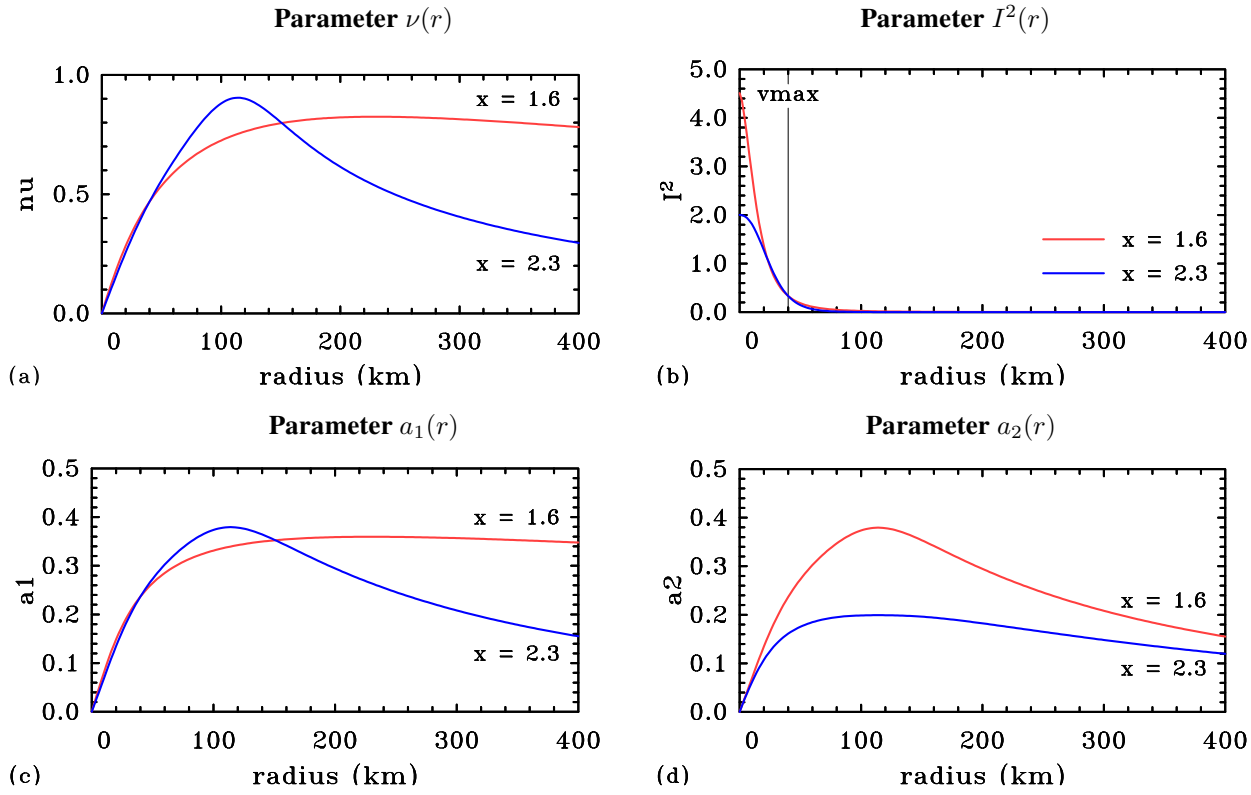

Figure 6. Radial variation of (a) ν, (b) I^2, (c) a_1 and (d) a_2. Curves for $x = 1.6$ in red, for $x = 2.3$ in blue.

the parameter ν, the drag coefficient multiplied by the boundary layer Reynolds' number, lies within the range 0 to 1 (panel (a)), as do the profiles of a_1 and a_2 that appear in the solutions (7), (8) and (15) (panels (c) and (d)). The profiles of a_1 have the same qualitative behaviour as those of ν, starting with a value of zero at $r = 0$. For $x = 1.6$, the profiles show a broad maximum near $r = 220$ km, beyond which they slowly decline. For $x = 2.3$, the maximum is more peaked near $r = 120$ km and they decline more rapidly, much like both profiles of a_2. Since the coefficients a_1 and a_2 appear in the combination $a_2 \cos(z/\delta) - a_1 \sin(z/\delta)$ in the solution for $u(r, z)$ in Equation (8), their individual contribution to $u(r, z)$ will vary with height.

Figure 6b shows the radial variation of the inertial stability, I^2, illustrating the rapid increase with decreasing radius inside the radius of maximum gradient wind and the fact that the broader vortex has a larger increase than the narrower vortex.

References

Abarca, S. F., M. T. Montgomery, and J. C. McWilliams, 2015: The azimuthally-averaged boundary layer structure of a numerically simulated major hurricane. *J. Adv. Model. Earth Syst.*, **07**, 10.1002/.

Anthes, R. A., 1971: Iterative solutions to the steady-state axisymmetric boundary-layer equations under an intense pressure gradient. *Mon. Wea. Rev.*, **99**, 261–268.

— 1974: The dynamics and energetics of mature tropical cyclones. *Rev. Geophys. Space Phys.*, **12**, 495–522.

Bell, M. M., M. T. Montgomery, and K. A. Emanuel, 2012: Air-sea enthalpy and momentum exchange at major hurricane wind speeds observed during CBLAST. *J. Atmos. Sci.*, **69**, 3197–3222.

Braun, S. A. and W.-K. Tao, 2000: Sensitivity of high-resolution simulations of Hurricane Bob (1991) to planetary boundary layer parameterizations. *Mon. Wea. Rev.*, **128**, 3941–3961.

Eliassen, A., 1951: Slow thermally or frictionally controlled meridional circulation in a circular vortex. *Astroph. Norv.*, **5**, 19–60.

— 1971: On the Ekman layer in a circular vortex. *J. Meteor. Soc. Japan*, **49**, 784–789.

Eliassen, A. and M. Lystad, 1977: The Ekman layer of a circular vortex: A numerical and theoretical study. *Geophys. Norv.*, **31**, 1–16.

Emanuel, K. A., 2018: 100 years of progress in tropical cyclone research. *Meteorological Monographs*, **59**, 15.1–15.68.

Kepert, J. D., 2001: The dynamics of boundary layer jets within the tropical cyclone core. Part I: Linear theory. *J. Atmos. Sci.*, **58**, 2469–2484.

— 2006: Observed boundary-layer wind structure and balance in the hurricane core. Part II. Hurricane Mitch. *J. Atmos. Sci.*, **63**, 2194–2211.

— 2013: How does the boundary layer contribute to eyewall replacement cycles in axisymmetric tropical cyclones? *J. Atmos. Sci.*, **70**, 2808–2830.

— 2017: Time and space scales in the tropical cyclone boundary layer, and the location of the eyewall updraft. *J. Atmos. Sci.*, **74**, 3305–3323.

Kepert, J. D. and D. S. Nolan, 2014: Reply to "comments on how does the boundary layer contribute to eyewall replacement cycles in axisymmetric tropical cyclones?. *J. Atmos. Sci.*, **71**, 4692–4701.

Kepert, J. D. and Y. Wang, 2001: The dynamics of boundary layer jets within the tropical cyclone core. Part II: Nonlinear enhancement. *J. Atmos. Sci.*, **58**, 2485–2501.

Kilroy, G., M. T. Montgomery, and R. K. Smith, 2017: The role of boundary-layer friction on tropical cyclogenesis and subsequent intensification. *Quart. Journ. Roy. Meteor. Soc.*, **143**, 2524–2536.

Kilroy, G., R. K. Smith, and M. T. Montgomery, 2016: Why do model tropical cyclones grow progressively in size and decay in intensity after reaching maturity? *J. Atmos. Sci.*, **73**, 487–503.

McWilliams, J. C., 1971: *The boundary layer dynamics of symmetric vortices*. Ph.D. thesis, Harvard University, University Microfilm, Inc., Ann Arbor, MI 48104, 89pp.

Montgomery, M. T. and R. K. Smith, 2017: Recent developments in the fluid dynamics of tropical cyclones. *Annu. Rev. Fluid Mech.*, **49**, 541–574.

Montgomery, M. T., H. D. Snell, and Z. Yang, 2001: Axisymmetric spindown dynamics of hurricane-like vortices. *J. Atmos. Sci.*, **58**, 421–435.

Montgomery, M. T., J. A. Zhang, and R. K. Smith, 2014: An analysis of the observed low-level structure of rapidly intensifying and mature Hurricane Earl (2010). *Quart. Journ. Roy. Meteor. Soc.*, **140**, 2132–2146, doi:10.1002/qj.2283.

Nguyen, C. M., R. K. Smith, H. Zhu, and W. Ulrich, 2002: A minimal axisymmetric hurricane model. *Quart. Journ. Roy. Meteor. Soc.*, **128**, 2641–2661.

Nolan, D. S., J. A. Zhang, and D. P. Stern, 2009a: Evaluation of planetary boundary layer parameterizations in tropical cyclones by comparison of insitu observations and high-resolution simulations of Hurricane Isabel (2003). Part I: Initialization, maximum winds, and the outer core boundary layer. *Mon. Wea. Rev.*, **137**, 3651–3674.

— 2009b: Evaluation of planetary boundary layer parameterizations in tropical cyclones by comparison of insitu observations and high-resolution simulations of Hurricane Isabel (2003). Part II: Inner core boundary layer and eyewall structure. *Mon. Wea. Rev.*, **137**, 3675–3698.

Persing, J., M. T. Montgomery, J. McWilliams, and R. K. Smith, 2013: Asymmetric and axisymmetric dynamics of tropical cyclones. *Atmos. Chem. Phys.*, **13**, 12299–12341.

Rayleigh, L., 1917: On the dynamics of revolving fluids. *Proc. Royal Soc. London. A*, **93**, 148–154.

Sanger, N. T., M. T. Montgomery, R. K. Smith, and M. M. Bell, 2014: An observational study of tropical-cyclone spin-up in supertyphoon Jangmi from 24 to 27 September. *Mon. Wea. Rev.*, **142**, 3–28.

Shapiro, L. J., 1983: The asymmetric boundary layer under a translating hurricane. *J. Atmos. Sci.*, **40**, 1984–1998.

Shapiro, L. J. and H. Willoughby, 1982: The response of balanced hurricanes to local sources of heat and momentum. *J. Atmos. Sci.*, **39**, 378–394.

Smith, R. K. and M. T. Montgomery, 2008: Balanced depth-averaged boundary layers used in hurricane models. *Quart. Journ. Roy. Meteor. Soc.*, **134**, 1385–1395.

— 2017: Comments on nonlinear response of a tropical cyclone vortex to prescribed eyewall heating with and without surface friction in TCM4: Implications for tropical cyclone intensification. *J. Atmos. Sci.*, 5101–5103.

Smith, R. K., M. T. Montgomery, and S. V. Nguyen, 2009: Tropical cyclone spin up revisited. *Quart. Journ. Roy. Meteor. Soc.*, **135**, 1321–1335.

Smith, R. K. and G. L. Thomsen, 2010: Dependence of tropical-cyclone intensification on the boundary-layer representation in a numerical model. *Quart. Journ. Roy. Meteor. Soc.*, **136**, 1671–1685.

Smith, R. K. and S. Vogl, 2008: A simple model of the hurricane boundary layer revisited. *Quart. Journ. Roy. Meteor. Soc.*, **134**, 337–351.

Smith, R. K., J. A. Zhang, and M. T. Montgomery, 2017: The dynamics of intensification in an HWRF simulation of Hurricane Earl (2010). *Quart. Journ. Roy. Meteor. Soc.*, **143**, 293–308.

Vogl, S. and R. K. Smith, 2009: Limitations of a linear model for the hurricane boundary layer. *Quart. Journ. Roy. Meteor. Soc.*, **135**, 839–850.

Willoughby, H. E., 1979: Forced secondary circulations in hurricanes. *J. Geophys. Res.*, **84**, 3173–3183.

— 1988: The dynamics of the tropical cyclone core. *Aust. Meteor. Mag.*, **36**, 183–191.

— 1995: Mature structure and motion. *Chapter 2 of A global view of tropical cyclones. (Ed. R. L. Elsberry), World Meteorological Organization, Geneva*, 21–62.

Zhang, D.-L., Y. Liu, and M. K. Yau, 2001: A multi-scale numerical study of Hurricane Andrew (1992). Part IV: Unbalanced flows. *Mon. Wea. Rev.*, **61**, 92–107.

Zhang, J. A., F. D. Marks, M. T. Montgomery, and S. Lorsolo, 2011: An estimation of turbulent characteristics in the low-level region of intense Hurricanes Allen (1980) and Hugo (1989). *Mon. Wea. Rev.*, **139**, 1447–1462.

Zhang, J. A. and R. F. Rogers, 2019: Effects of parameterized boundary layer structure on hurricane rapid intensification in shear. *Mon. Wea. Rev.*, **147**, 853–871.

Zhang, J. A., R. F. Rogers, D. S. Nolan, and V. Tallapragada, 2015: Evaluating the impact of improvements in the boundary layer parameterization on hurricane intensity and structure forecasts in HWRF. *Mon. Wea. Rev.*, **143**, 3136–3155.

Zhang, J. A., R. F. Rogers, and V. Tallapragada, 2017: Impact of parameterized boundary layer structure on tropical cyclone rapid intensification forecasts in HWRF. *Mon. Wea. Rev.*, **145**, 1413–1426.

